

ADVANCED EXPERIMENTAL AND NUMERICAL ANALYSIS OF A PRESSURIZED AIR WAVE BEARINGS

Adrian Sescu,
University of Toledo, Toledo, OH

Florin Dimofte,
University of Toledo at NASA GRC, Cleveland, OH

Carmen Sescu,
University of Toledo, Toledo, OH

Abdollah A. Afjeh,
University of Toledo, Toledo, OH

Robert Handschuh,
The Army Research Laboratory, Cleveland, OH

ABSTRACT

Experimental, analytical, and numerical investigations have been done in the field of gas lubrication, but few people focused on details of fluid flow between the sliding surfaces. In this work the entire pressurized wave bearing is analyzed in detail. The numerical study using a three-dimensional commercial code and a two-dimensional finite difference code gives information about the flow at many levels. The numerically computed flow rates using the commercial code are compared with experimental results determined at NASA Glenn Research Center on an experimental rig. The calculated discharge coefficient is used in the finite difference code which solves the Reynolds equation. The holes effect is considered as a source term, instead of applying hybrid type boundary conditions on the holes contours. Data from experimental tests, commercial three-dimensional code, and two-dimensional code are reported and compared to each other. Good agreement was found between numerical study and experiment.

INTRODUCTION

Due to compressibility of the fluid, the understanding of the mechanisms of gas lubrication is different from those of the liquid based lubrication. The presence of supply holes for pressurization increases the complexity of the problem. Helene et. al [1,2] performed a numerical computation of a three-dimensional compressible flow inside a hybrid journal bearing. Useful details of the flow in the vicinity of the supply holes can be found in these results. They found no significant recess flow pressure due to Mach number, and also revealed that the inclination of the holes axes could visibly change the three-dimensional pressure distribution. He et al [3] analyze the influence of the orifice geometry on the journal bearing

properties by using a three dimensional code to predict the discharge coefficient. San Andres et al [4] predict the bearing properties by integrating the film averaged momentum transport and energy equations combined with turbulence models. Their numerical results were compared to experimental data.

In this paper, a pressurized wave bearing (see Dimofte [5,6]) is investigated. First, a commercial code that analyzes the flow in the vicinity of the entrance to fluid film is used. The discharge coefficient calculated with this code, is then used as an input for a numerical code that efficiently predicts the steady-state performance of the pressurized air wave bearing. The theoretical results are compared to test data obtained at NASA Glenn Research Center.

RESULTS

Three-dimensional problem

As a first step, the three-dimensional solver integrates the laminar equations for a prediction of the Reynolds number (Fig. 1). Three different possible regimes (laminar, transition and turbulent) are identified. Then the laminar and the Reynolds Averaged Navier Stokes (RANS) [7] equations are again integrated. Spalart – Almaras [8] turbulence model is used for the transition flow. Similarly, Jones and Launder $k-\epsilon$ turbulence model is introduced to deal with turbulent zones. The geometry of three discretized holes of the wave bearings is illustrated in Fig. 2. Inside the holes and in the film (around the holes), radial symmetry of cells distribution was used. In the vicinity of the entrance to the film the grid was stretched to capture the flow in more detail. Five cells were used across the film thickness. Five types of boundary conditions were

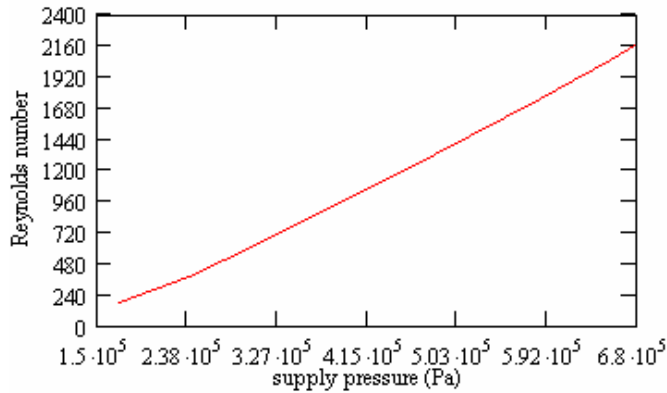


Fig. 1 Local Reynolds number at the entrance to the fluid film vs. supply pressure.

considered: pressure inlet for inflow boundary, pressure outlet for outflow boundary, wall (no-slip), symmetry at the bearing centerline, and periodic conditions for circumferential direction. The supply pressure gauge was varied between 0.7 and 5.5 MPa (10 - 80 PSI). Depending on grid configuration, a test case for the solver may take about 10-20 minutes.

For high supply pressures (greater than 60 PSI gauge), the flow may become turbulent in the vicinity of the film entrance. Following the concept of local isotropy proposed by

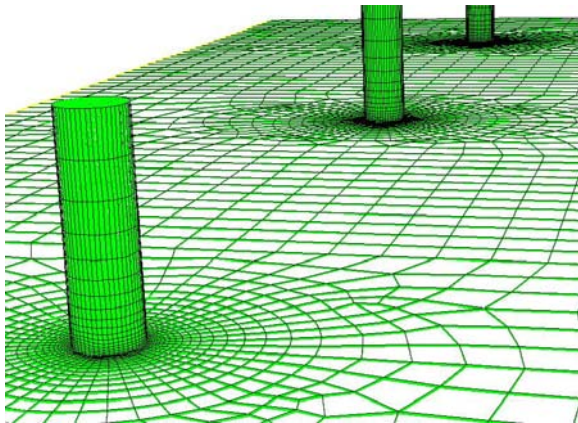


Fig. 2 Discretization detail of a pressurized hole.

Kolmogorov [8], because the film thickness is very small and approaches the relatively small scales of turbulence, any permanent sense of turbulence direction is lost. As a result, the effect of predicted turbulence over the global properties of the flow is weak, and could be neglected.

Reynolds number vs. supply pressure in Fig. 1 represents the fluid film away from the hole; it uses the film's thickness as characteristic length. In the vicinity of the film entrance the characteristic length can switch to the diameter of the hole. As a result, the magnitude of Reynolds number can be much higher due to the ratio between hole's diameter and film's thickness (the ratio may reach 35). Based on Fig. 1, inside the film weak instabilities may occur. In the vicinity of the entrance to the film the flow may become fully turbulent (as it was

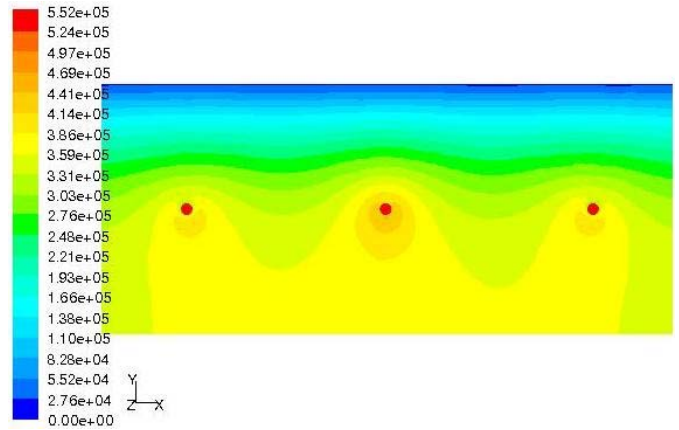


Fig. 3 Pressure contours (PSI) at the surface of the shaft for a supply pressure gauge of 5.5 MPa (80 PSI).

pointed above, the Reynolds number may reach high values, the order of 10^4). For this reason the solver uses turbulence modeling for high supply pressures.

In Fig. 3 the pressure distribution on the shaft is shown. The difference from hole to hole in the pressure distribution is due to the variation of the film thickness.

The flow rates obtained using the commercial code were then compared to the experimental data determined using a dedicated experimental rig at NASA Glenn Research Center for different supply pressures. The rig uses a commercial spindle capable of 30,000 RPM with a run-out of less than $1 \mu\text{m}$. The rig was set up with the shaft orientated vertically such that the test bearing could be easily set to run unloaded. The pressurization is done through two rows of 9 holes each. The

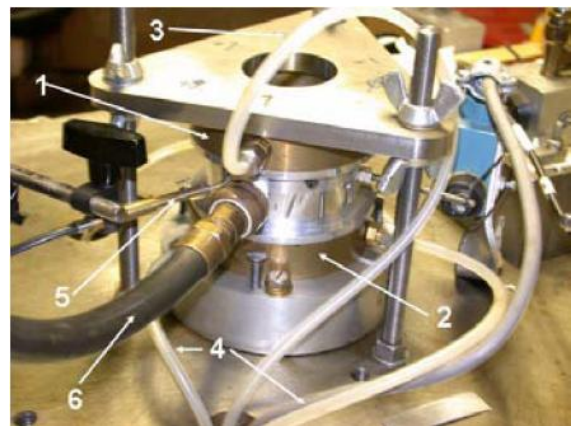


Fig. 5 Experimental rig located at NASA Glenn Research Center.

setup of the test bearing is shown in Fig. 5. The bearing housing is supported by two thrust levitating plates (Fig. 5, items 1 and 2), supply with air (3 and 4) that allows the bearing to move freely in the radial direction. Light beam proximity probes (5) are used to observe the bearing behavior. A flexible hose (6) pressurizes the bearing with air. Four sets of measurements were conducted corresponding to four different

angular velocities (0, 5000, 10000, and 15000 RPM). The plot

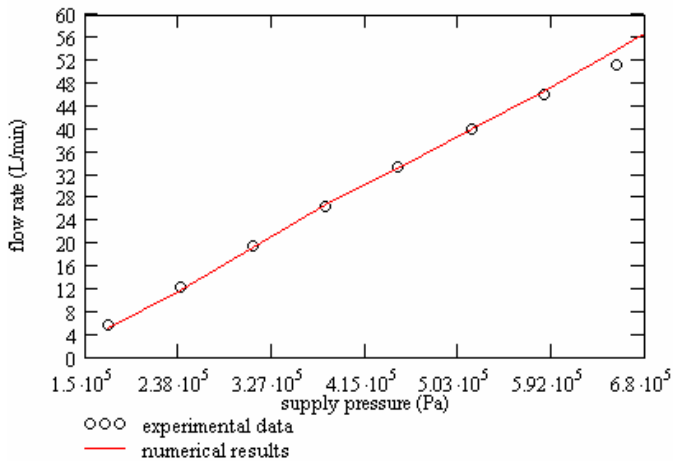


Fig. 6 Comparison between experimental and numerical flow rates.

showing the comparison between experimental and numerical results is given in Fig. 6 (the numerical curve may not be smooth because different models were used: laminar and turbulent). Good agreement was found between numerical study and experiment.

Comparison between the numerical flow rates and the experimental data is presented in Fig. 6.

Two-dimensional problem

The calculated discharge coefficient obtained with the commercial code is then used to integrate the quasi-linear

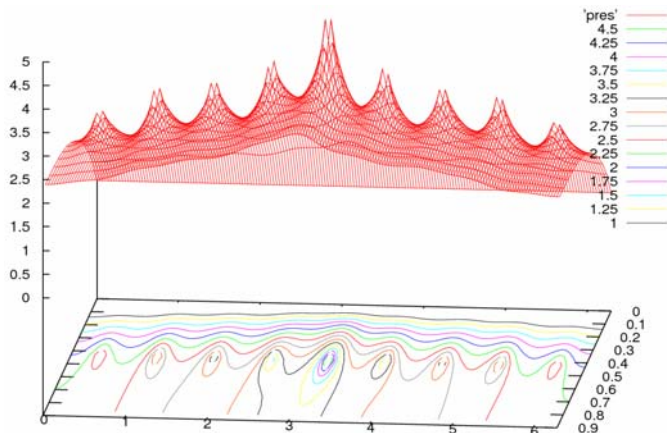


Fig. 7 Pressure distribution (PSI) surface for a supply pressure of 50 PSI gauge applied to the wave bearing (the wave amplitude is 0.2, and the dislocation is 0.4 from clearance).

unsteady Reynolds equation. Instead of applying hybrid type boundary conditions on the holes contour, a source term is introduced into the equation (see Czolczynski [9]). The Reynolds equation is discretized using a second order centered finite difference scheme (see Hoffmann [10]). A fourth order Runge Kutta (see Lomax [11]) method is used to integrate in time the Reynolds equation. The steady state solution is

determined with a 10E-6 accuracy. In order to avoid the oscillations in the large gradient regions, filtering techniques were introduced (see Kennedy and Carpenter [12]). The pressure distribution for a three wave journal bearing with a wave amplitude ratio of 0.2, an eccentricity of 0.4 and a supply pressure of 50 PSI is presented in Fig. 7. The components of the fluid film force are determined by integrating the pressure distribution over the entire film.

CONCLUSIONS

Numerical results for a steady state analysis of a pressurized wave bearing were provided by a commercial and a two-dimensional code. The numerical predictions were compared to test data. Good agreement was found between them.

REFERENCES

- [1] Helene, M., Arghir, M., and Frene, J., 2003, "Numerical Three-Dimensional Pressure Patterns in a Recess of a Turbulent and Compressible Hybrid Journal Bearing," *J. of Trib.*, **125**(2), pp. 301-308.
- [2] Helene, M., Arghir, M., and Frene, J., 2005, "Combined Navier-Stokes and Bulk-Flow Analysis of Hybrid Bearings: Radial and Angled Injection," *J. of Trib.*, **127**(2), pp. 557-367.
- [3] He, M., Song, X., Allaire, P., and Cloud, C. H., 2005, "Hydrostatic Bearing Performance Considering Orifice Geometry Effects," *STLE 60th Annual Meeting*, Las Vegas, Nevada.
- [4] San Andres, L., Childs, D., and Yang, Z., 1995, "Turbulent-Flow Hydrostatic Bearings: Analysis and Experimental Results," *J. of Trib.*, **125**(2), pp. 301-308.
- [5] Dimofte, F., and Hendricks, R. C., 2002, "Wave Journal Bearing under Dynamic Loads," *NASA/TM-2002-211079*.
- [6] Dimofte, F., Cioc, S., Handschuh, R. F., and Fleming, D. P., 2005, "On The Influence of the Supply Pressure on the Dynamic Stability of Hybrid Gas Journal Wave Bearings," *Proceedings of WTC2005 World Tribology Congress III*, Washington, D.C., USA.
- [7] Deissler, R. G., 1998, "Turbulent Fluid Motion," *Taylor & Francis*, Philadelphia, USA.
- [8] Wilcox, D. C., 2002, "Turbulence Modeling for CFD," *D C W Industries*.
- [9] Czolczynski, K., 1999, "Rotordynamics of Gas-Lubricated Journal Bearing Systems," *Springer-Verlag*.
- [10] Hoffmann, K. A., and Chiang, S. T., 2000, "Computational Fluid Dynamics for Engineers," 4th ed., *Engineering Education Systems*.
- [11] Lomax, H., Pulliam, T. H., and Zingg, D. W., 2005, "Fundamentals of Computational Fluid Dynamics," *Springer-Verlag*.
- [12] Kennedy, C. A., and Carpenter, M. H., 1997, "Comparison of Several Numerical Methods for Simulation of Compressible Shear Layers," *NASA Technical Paper*, 3484